Available online at www.sciencedirect.com

SciVerse ScienceDirect

Ceramics International 39 (2013) 8227–8235

CERAMICS INTERNATIONAL

www.elsevier.com/locate/ceramint

Macrostructures with hierarchical porosity produced from alumina–aluminum hydroxide–chitosan wet-spun fibers

Rafael Salomão[a,*], Jamile Brandi[b]

[a]Materials Engineering Department, São Carlos School of Engineering, University of São Paulo, Avenida Trabalhador São-carlense, 400 13566-590 São Carlos, SP, Brazil

[b]Federal University of the ABC Region (UFABC), Rua da Catequese, 242 09090-400 Santo André, SP, Brazil

Received 8 March 2013; received in revised form 28 March 2013; accepted 2 April 2013
Available online 10 April 2013

Abstract

This paper reports on the development of macrostructures with hierarchical porosity produced from Al_2O_3–$Al(OH)_3$–chitosan wet-spun fibers. Aqueous suspensions (13 vol% of solids, 1.3 vol% of chitosan, 0.1 M acetic acid, pH–4) containing different Al_2O_3–$Al(OH)_3$ ratios were extruded through a 500 μm diameter syringe needle into a 2 M NaOH coagulation bath. After washing and drying, these continuous fibers were controllably chopped into 5 mm long staples and shaped under vacuum into 40×40 mm^2 cylindrical macroelements, using 2 wt% chitosan solution as binder. By varying the Al_2O_3–$Al(OH)_3$ content (100–0, 50–50 and 0–100 vol%) and sintering temperature (1100–1500 °C), structures with different levels of porosity (up to 84%), specific surface area (up to 7 m^2 g^{-1}) and mechanical strength (up to 9 MPa in uniaxial compression) were obtained. The ratio between the porosity inside the solid part of the structure and the interfilament space was also affected by these parameters and was adjusted according to the numerous potential applications of this system.

Keywords: Hierarchical structure; Gelcasting; Porous; Fibers; Spinning

1. Introduction

Ceramic materials with hierarchical porosity, i.e., organized in different levels [1,2], have an interesting synergy of properties and characteristics, as shown by the following examples: (1) Filtering elements containing multimodal pore size distribution combine (i) fine and ultrafine pores with great capacity for sieving hazardous compounds and removing small impurities (such as bacteria and microparticles), and (ii) larger macroscopic ones with high permeability and cleaning ability [3]. (2) High-temperature insulation bricks show low interconnectivity among the pores (to prevent hot air convection) and suitable mechanical strength (to withstand thermal shock stresses) [3,4]. (3) Biological scaffolds have pores with smooth internal surfaces that facilitate cell settling and growth [5]. Different processing methodologies have been proposed to produce these types of structures. Cellular structures with a narrow pore size distribution and low interconnectivity are produced using surfactant agents (organic and inorganic solid nanoparticles) to stabilize foamed ceramic suspensions [4]. Wood and paper-like cellulose-based sacrificial templates combined with colloidal ceramic particles produce bio-mimicked porous structures [6,7]. Other examples include ice-templated structures [8], extrusion-oriented pores [9], heterocoagulation of colloidal organic particles [10] and three-dimensional printing [11,12].

Recent studies have demonstrated the possibility of producing porous structures using wet-spun ceramic fibers [13–17], which, after compacting and sintering, exhibit two levels of porosity: microscopic, inside the fibers' microstructure (intrafiber), and macroscopic, comprising the space between the filaments (interfiber). In these cases, the intrafiber porosity is formed by packing flaws among the particles and by the decomposition of the organic binders employed in their consolidation [17], generating only a limited content of intrafiber pores. However, if another porogenic agent were introduced in the fibers' composition, it is reasonable to assume that high levels of porosity would be produced. To evaluate this hypothesis, this paper describes how filamentous macroporous structures have been produced using calcined alumina

*Corresponding author. Tel.: +55 16 33739576; fax: +55 16 33739590.
E-mail addresses: rsalomao@sc.usp.br (R. Salomão), jamilebrandi@gmail.com (J. Brandi).

0272-8842/$ - see front matter © 2013 Elsevier Ltd and Techna Group S.r.l. All rights reserved.
http://dx.doi.org/10.1016/j.ceramint.2013.04.007

(CA, α-Al_2O_3) as the main component of the fibers, aluminum hydroxide (AH, $Al(OH)_3$) as a porogenic agent, and chitosan as a binding agent.

The CA–AH system was chosen for this study due to four important technological advantages: (1) in aqueous suspensions, CA–AH mixtures can be easily dispersed under the same conditions (pH range and dispersant additive) due to their chemical similarity [18,19]; (2) it can be processed by many different methods and is compatible with most of the hydraulic binders employed in the refractory industry (calcium aluminate cement, hydratable alumina, colloidal binders and gelcasting) [20]; (3) after firing (up to 1200 °C), the transition phases observed from the $Al(OH)_3$ decomposition result in highly refractory α-Al_2O_3 [21–23]; and (4) both raw materials are abundant worldwide and show competitive costs. Chitosan, an abundant natural renewable polysaccharide, was selected as a binding agent because of its high compatibility with alumina-based particles, excellent mechanical properties and eco-friendly appeal [24–27].

The most suitable conditions to produce stable aqueous CA–AH–chitosan suspensions were initially determined based on Zeta potential and turbidity versus pH measurements. These suspensions were wet-spun as thin continuous fibers with different CA/AH ratios, using chitosan as a gelcasting binding agent. After drying, the fibers were compacted into cylindrical macrostructures, fired at different temperatures (1100–1500 °C) and tested for porosity, specific surface area and mechanical strength. Scanning electron microscopy was employed to evaluate their microstructural changes.

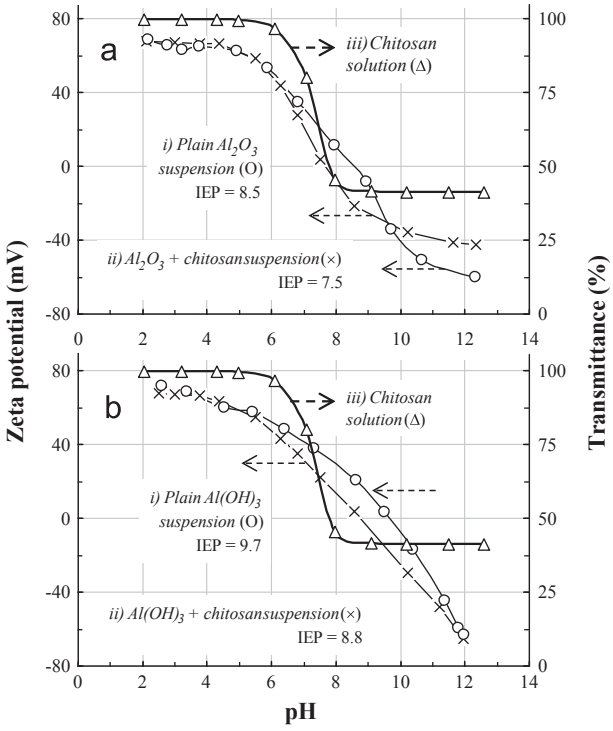

Fig. 1. Zeta potential (ZP) versus pH behavior for (a) CA plain and CA–chitosan suspensions and (b) AH plain and AH–chitosan suspensions. The effect of pH on chitosan solubility (at 25 °C) evaluated by transmittance measurements [28] is also shown for comparison.

2. Preparation of the CA/AH–chitosan fibers

2.1. Preparation of the Al_2O_3–$Al(OH)_3$–chitosan precursor suspensions

The first step in the preparation of aqueous suspensions containing different types of solid particles and dissolved polymers is to ensure that they have the same charges (positive or negative), so that they can be dispersed in the same pH range. This condition was evaluated based on zeta potential measurements (DT-1202, Dispersion Technology Inc., US) for the solid particles and turbidity tests (UV–vis spectrophotometer Carry 50, Varian) for chitosan (97% deacetylation, Polymar, Brazil), versus pH (Fig. 1). Properties of the raw materials employed in the tests are shown in Table 1.

Using a 0.1 M acetic acid solution, calcined alumina (CA, CT 3000 SG, Almatis, Germany) or aluminum hydroxide (AH, Hydral 710, Almatis, Germany) suspensions (2 vol% of solids) were prepared in a paddle mixer and sonicated for 2 min to improve particle individualization. The pH was shifted continuously toward alkaline ranges using a 0.5 M NH_4OH solution, with a 1-minute interval between each measurement for stabilization. Similar suspensions containing 2 vol% of solids and a chitosan-solid ratio of 9 vol% were tested in the same conditions.

The water-solubility of chitosan is strongly dependent on pH and was evaluated in turbidity tests using a UV–vis spectrophotometer (Carry 50, Varian, quartz cell with 1 cm optical path length at 600 nm) [28]. The chitosan solution (2 wt% of chitosan in 0.1 M acetic acid solution, pH 4) was prepared by stirring it at 40 °C, for 24 h, until the polymer was completely dissolved. Concentrated NaOH was added to shift the pH while the transmittance of the solution was being recorded.

Due to their chemical similarity, CA and AH suspensions showed a similar pH range for suitable dispersion, i.e., below 6 (positive charge) and above 11 (negative charge), at which they show highly charged particle surfaces. Chitosan, on the other hand, as described elsewhere [28] behaves as stable dissolved positively charged polyelectrolyte only in acid pH (below 6) and achieves the highest transmittance levels (for pH > 6, charges are neutralized and it precipitates). Therefore, a 0.1 M acetic acid solution with pH 4 is a favorable medium for co-dispersion and preparation of high CA–AH load chitosan-containing suspensions (Fig. 1a–b), as described in the next section.

2.2. Wet-spinning of the fibers

For the preparation of the CA/AH–chitosan suspensions for gelcasting extrusion, compositions containing CA and AH were initially dry-blended: 100 wt% Al_2O_3 (100CA_000AH), 50 wt% Al_2O_3 (050CA_050AH) and 100 wt% $Al(OH)_3$ (000AC_100AH). They were dispersed in a 0.1 M acetic acid

Table 1
Properties of the raw materials employed in the tests.

	Calcined alumina (CA)[a]	Aluminum hydroxide (AH)[b]
Chemical analysis (wt%; typical values)	α-Al_2O_3: 99.78; Na_2O: 0.08; Fe_2O_3: 0.02; SiO_2: 0.03; CaO: 0.02; MgO: 0.07	$Al(OH)_3$: 99.7; Na_2O: 0.256; Fe_2O_3: 0.007; SiO_2: 0.004
Specific surface area (BE ; $m^2\ g^{-1}$)	7.2 ± 1.0	4.2 ± 1.0
Particle size (μm; D_{50}/ D_{90})	0.61/0.95	0.89/0.98
Density (Helium pycnometry; $g\ cm^{-3}$)	3.96 ± 0.05 (before firing)	2.42 ± 0.05
Isoelectric point (pH; dispersant-free)	8.5	9.7
Loss of ignition (LOI, %, at 1000 °C)	0.81	34.9
[c]Chitosan		
Molecular weight (M_N, $g\ mol^{-1}$)	54.350	
Deacetylation degree (%)	97	
Water solubility (pH range, at 25 °C)	≤6 (28)	
Loss of ignition (%, 1000 °C)	97.3 (Fig. 4a)	
Thermal decomposition (°C, T_{90}–T_{10})	219–505	

[a]CT3000SG, Almatis, Germany.
[b]Hydral 710, Almatis, Germany.
[c]Polymar, Brazil.

solution (40 vol% of solids, pH 4) in a ball mill (2 h, at 60 rpm, using a 10:1 ratio of 10 mm zirconia spheres) (Fig. 2a). The chitosan solution (2 wt% of chitosan in 0.1 M acetic acid solution, pH 4) was prepared by stirring it at 40 °C, for 24 h, until the polymer dissolved completely (Fig. 2b). Identical volumes of the 2 wt% chitosan solution and CA–AH suspensions were mixed in a paddle mixer for 10 min at 100 rpm (Fig. 2c) to produce a system containing 13 vol% of solids and 1.3 vol% of dissolved organics (after drying, the chitosan content in the system increases to 9.1 vol%) (Table 2).

The CA/AH–chitosan suspensions were then poured into a syringe connected to an air compressor (constant pressure of 30 kN m^{-2}, Fig. 2d). The tip of its needle (500 μm diameter × 10 mm length) was inserted under the surface of a stirring 10 °C 2 M NaOH solution (pH 14). After the first contact between the suspension and the alkaline medium, the pH increased rapidly to above 6, generating a combination of two effects, shown in Fig. 1, which consolidated the system. (1) The addition of chitosan shifted the CA and AH isoelectric points (IEP) to lower pH values (from 8.5 to 7.5 and from 9.7 to 8.8, respectively) and reduced the zeta potential levels attained at pH values above 9, due to a mutual partial charge neutralization. This effect indicates that, when pH is shifted above 6, chitosan solubility is reduced and the CA/AH particles, that became less positively charged, behave as an adsorption site for these molecules [24]. (2) The contact between the extruded suspension and the cool and alkaline coagulation bath causes chitosan to precipitate as gel due to the deprotonation of the $(R–NH_3)^+$ groups, further restricting particle mobility[15,17]. Because this consolidation mechanism occurs almost instantaneously, the initial shape the suspension assumes upon contact with the coagulation bath is preserved and beads are produced [15] by dripping the suspension. On the other hand, by inserting the tip of the needle into the solution, the extrusion of the suspension generated 300–500 μm diameter continuous fibers (Fig. 2e) [14,16,17].

After soaking in the solution for 1 h for complete coagulation, the fibers were washed until pH was neutral and dried at 80 °C for 24 h (Fig. 2f and g). Their aspect is depicted in Fig. 3a.

3. Preparation and characterization of the porous filamentous macroelements

3.1. Compacting and sintering of CA/AH-chitosan fibers

To produce the filamentous macroelements, initially, the continuous dried green fibers were reduced to staples of approximately 5 mm in a rotating plastic cylinder (diameter = 10 cm, height = 30 cm, 60 rpm, without milling elements) for 60 min (Figs. 2h and 3b). These staples were then vibration compacted in a cylindrical non-adherent mold (diameter = 40 mm, height = 40 mm), where 2 wt% of chitosan were poured into 0.1 M acetic acid solution, filling the spaces (Fig. 2i). Vacuum filtering and 80 °C drying overnight were then applied to remove the excess of chitosan solution and consolidate the structure, respectively.

Considering the many thermal reactions involved in the decomposition of chitosan and AH, the dried green fibers and their as-received constituent raw materials were analyzed by thermogravimetry (TGA-Q50, TA Instruments, 10 °C.min^{-1}, 25–800 °C, in synthetic air atmosphere).

The chitosan grade employed here (Fig. 4a) decomposes almost completely between 219 °C and 505 °C (in synthetic air condition, 97.8 wt%). Three events can be observed: release of free water up to 150 °C and two sequential stages of intense mass loss between 170–380 °C and 380–560 °C related, respectively, to the decomposition of the main polymeric chain and the final oxidation of the carbonaceous residues formed. The calcined alumina shows a slight mass loss (0.8 wt %) due to the dehydroxylation of its surface (Fig. 4b), whereas aluminum hydroxide decomposes between 200–400 °C, with a significant mass loss (34.9 wt%) (Fig. 4c). These behaviors

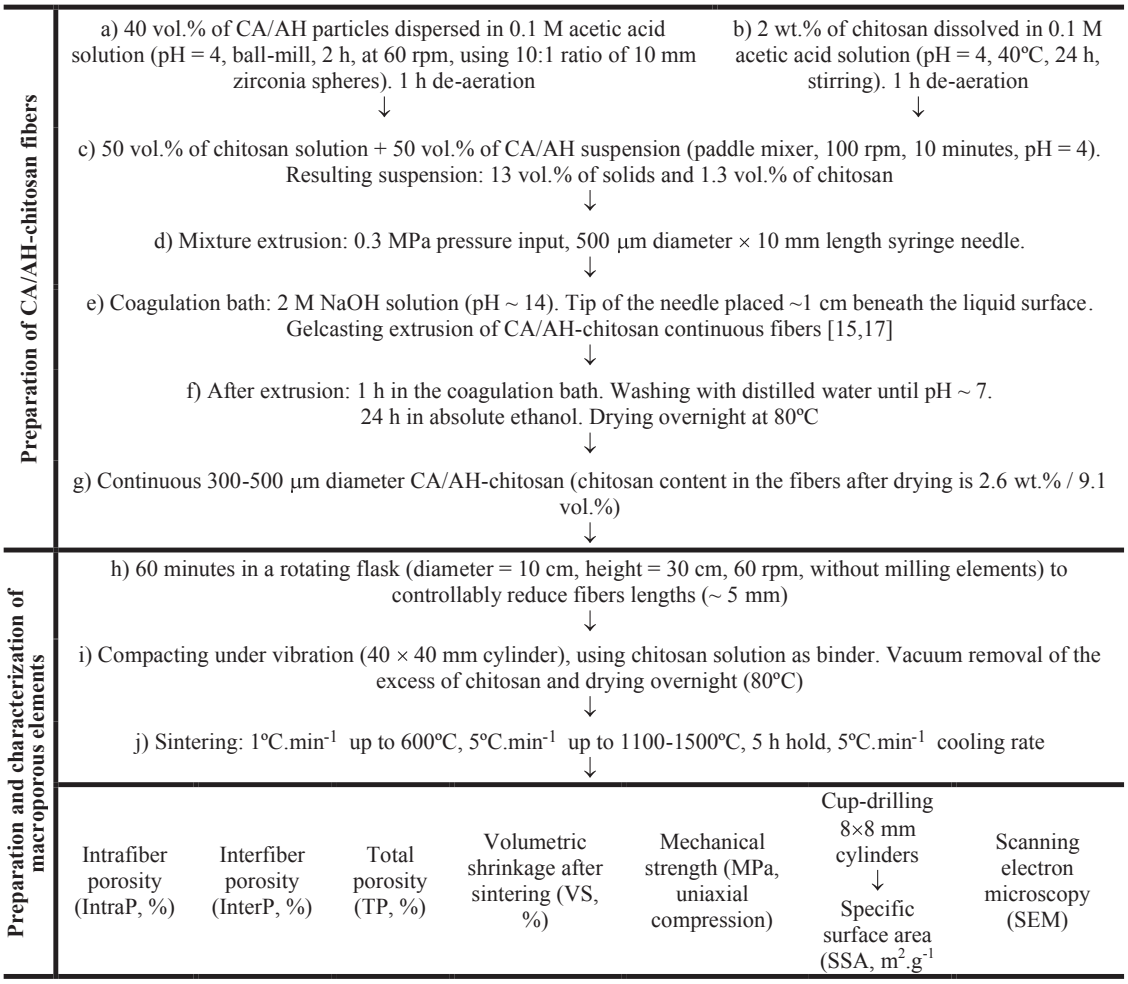

Fig. 2. Sequential representation of the fibers gelcasting extrusion (a–g) and preparation and characterization of the filamentous macroelements (h–j).

Table 2
Compositions tested.

		Alumina/$Al(OH)_3$+Chitosan mixtures			
CA-AH suspensions	CA/AH (wt%/wt%)	100CA000AH	100/0	40 vol%	50 vol%
		050CA050AH	50/50		
		000CA100HA	0/100		
	Acetic acid solution (0.1 M)	60 vol%			
Chitosan solution	Chitosan	2 wt%			50 vol%
	Acetic acid solution (0.1 M)	98 wt%			

are consistent with other reports published in the literature [21,29–31].

During the tests of the dried fibers (Fig. 5), decomposition of the low chitosan content did not significantly affect the mass loss profile of the CA–AH mixtures. Conversely, the dehydroxylation of AH caused intense mass loss within a relatively short temperature interval. These results justified the heating schedule employed to sinter the macroelements: 1 °C min^{-1} up to 600 °C, 5 °C min^{-1} up to the maximum temperature (1100–1500 °C), 5 h hold and 5 °C.min^{-1} cooling rate (Fig. 2j). The sintered macroelements are shown in Fig. 3c.

3.2. Characterization of the macroelements

As reported elsewhere [2,3] and schematically shown in Fig. 6, this type of filamentous porous structure comprises two main families of pores: (i) micropores inside the filaments ($D_{Pores} < 500$ μm) and (ii) macropores ($D_{Pores} \geq 500$ μm). The former are generated by particle packing flaws, organic particles and decomposition of hydroxides or carbonates [15,17], while the latter corresponds to the macroscopic interfilament spaces. There are significant differences in average pore size and pore content and in

Fig. 3. Dried green fibers (050CA050HA sample) (a) before and (b) after length reduction; (c) filamentous macrostructure attained (050CA050HA sample) after firing at 1500 °C.

the role of each family of pores in every possible application of these structures. Therefore, distinct characterization techniques must be employed to assess these different porosities. Five samples were tested in each of the following tests.

Initially, to measure the apparent microporosity inside the fibers, or intrafiber porosity (IntraP, %), the samples were

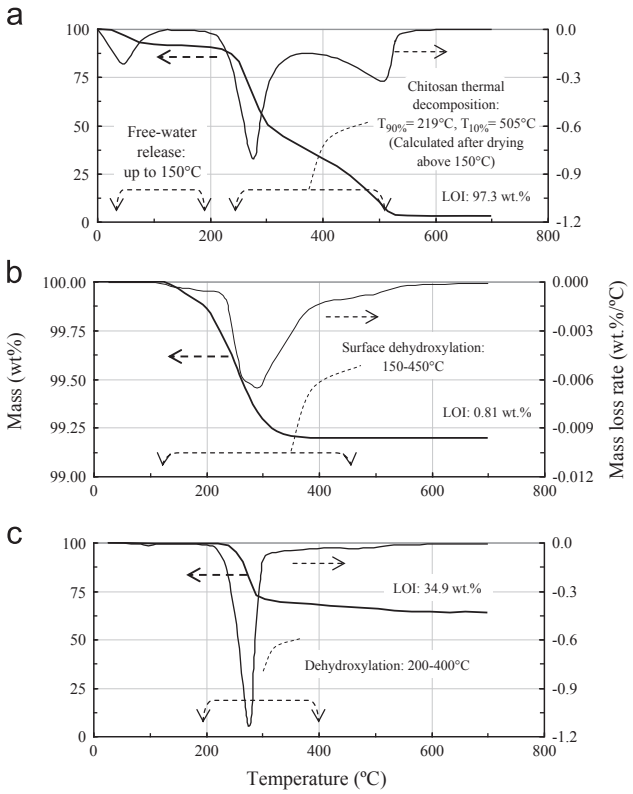

Fig. 4. Thermogravimetry of the raw materials employed in the tests: (a) chitosan, (b) calcined alumina (CA) and (c) aluminum hydroxide (AH).

characterized by the Archimedes method, using ethanol as immersion fluid. To ensure that only the pores inside the solid part were considered in this test, the excess ethanol between the fibers was removed carefully by applying a weak blast of compressed air before each mass recording. To calculate the structure's total porosity (TP, %) and macroporosity around the fibers, or interfiber porosity (InterP,%), other samples of each composition were weighed (M_S,g) and their external volume was measured (V_T,cm^3). The samples were then crushed ($D_{Particle} < 212$ μm) and the density of the solid part was measured (ρ_S, g cm^{-3}, helium pycnometry, Ultrapyc 1200e, Quantachrome Instruments, USA). The total (TP) and the interfiber (InterP) porosities of the macroelements were calculated by eqs. 1 and 2:

$$TP(\%) = 100\%(V_T - (M_S/\rho_S))/V_T \quad (1)$$

$$InterP(\%) = TP - IntraP \quad (2)$$

The volumetric shrinkage (VS,%) of the samples was calculated using eq. 3:

$$VS(\%) = 100\ \%(V_{Initial} - V_{Final})/V_{Initial} \quad (3)$$

where $V_{Initial}$ and V_{Final} are the samples' external volume before and after thermal treatment, respectively.

For specific surface area (SSA) measurements (BET method, Nova 1200e, Quantachrome Instruments, USA,

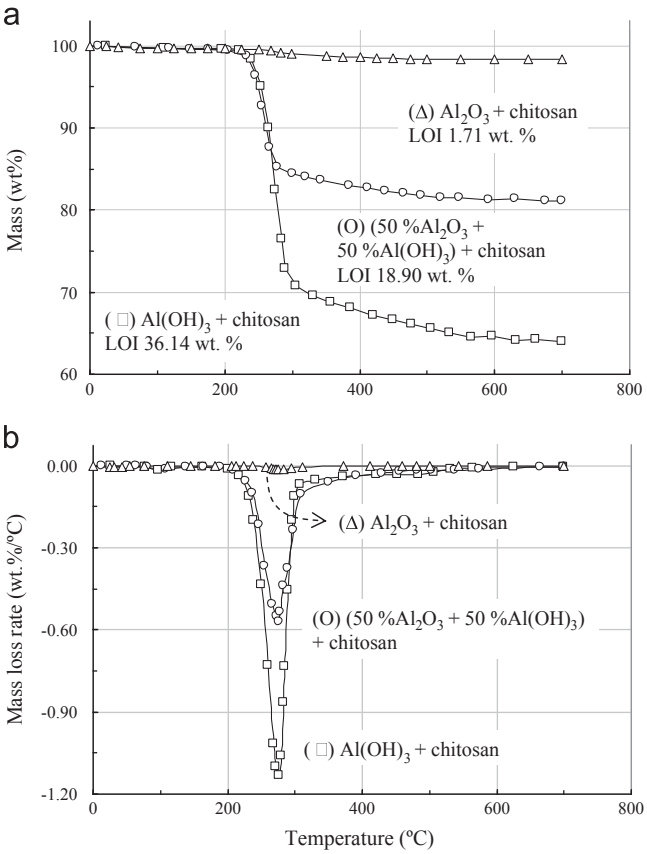

Fig. 5. Thermogravimetry of the green dried CA-chitosan, AH–chitosan and CA–AH–chitosan (050CA050HA sample) fibers: (a) mass loss and (b) mass loss rate.

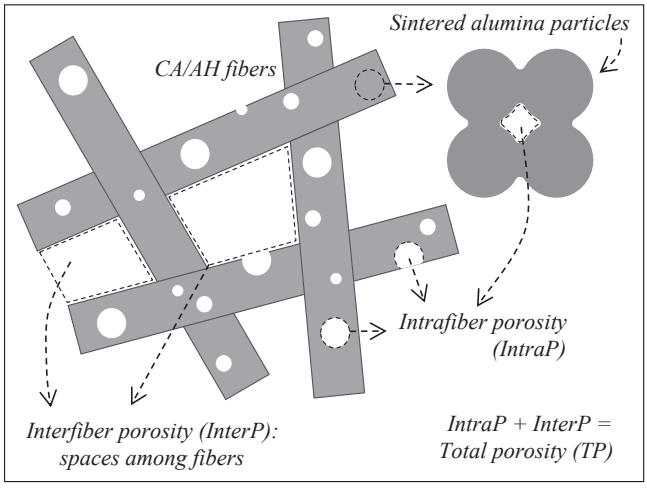

Fig. 6. Schematic representation of the pores inside the fibers structure (IntraP) and of those among the fibers (InterP).

ASTM C1069-09), $8 \times 8\ mm^2$ cylindrical specimens were extracted from the main sample using a cup bit drill and degassed for 2 h at 200 °C prior to each measurement. High purity nitrogen (99.999%) was used as the adsorption gas for the SSA measurements.

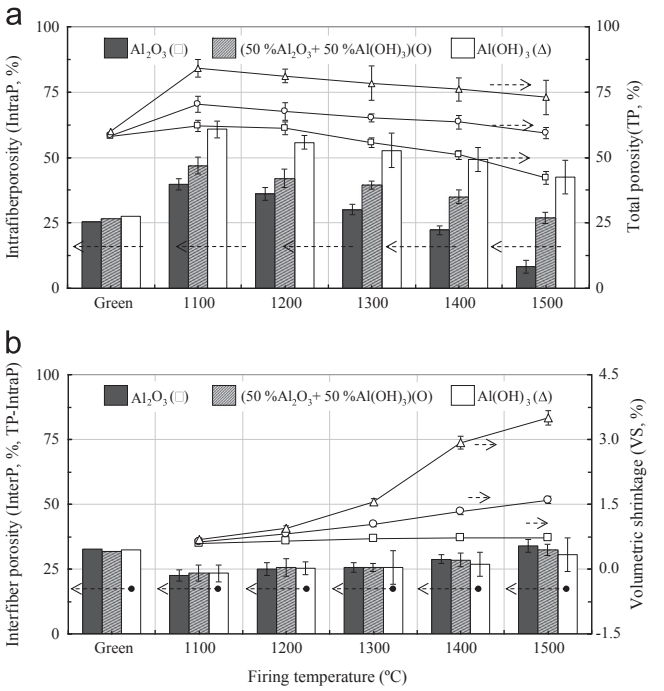

Fig. 7. Porosity results: (a) Intrafiber (IntraP) and total (TP) porosity and (b) Interfiber (InterP) and volumetric shrinkage (VS) of the macroelements fired at different temperatures.

The mechanical strength was measured under uniaxial compression, according to the ASTM C496-90 standard, in MTS 810 TestStar II tensile tester at a loading rate of $2\ N\ s^{-1}$. Seven samples were tested in each condition, and their microstructure was analyzed by scanning electron microscopy (SEM, Philips XL30 FEG. EHT = 7.00 kV)

3.2.1. Intrafiber porosity and specific surface area

The green samples showed similar IntraP, TP (Fig. 7a) and InterP (Fig. 7b) values. This result indicates that similar structures were produced after consolidation because the same processing method and volumetric amount of solids and chitosan were employed in all the compositions (Fig. 8a, b and 8c). Therefore, the variations in porosity observed after thermal treatment are more likely the result of changes induced by the decomposition of chitosan, $Al(OH)_3$ and sintering, leading to two important effects.

Previous investigations into calcined alumina and $Al(OH)_3$-based systems have found that the thermal decomposition of $Al(OH)_3$ occurs according to the general expression [21,30,32]:

Firstly, $Al(OH)_3$ decomposition is followed by a significant volumetric shrinkage of the particles due to the increase in density from $2.43\ g\ cm^{-3}$ up to $3.95–4.00\ g\ cm^{-3}$ (when heating above 400 °C). If these particles were previously inserted into a rigid calcined alumina matrix, this shrinkage would behave as an inorganic pore generator (Fig. 8d–f). Secondly, $Al(OH)_3$ (in the Gibbsite form) has a typical hexagonal metal hydroxide structure in which hydrogen bonds build up layers of hydroxyl groups, with aluminum ions occupying two-thirds of the octahedral holes between two of

these layers [31]. Upon heating the material above 220 °C, intense dehydroxylation causes the layers to collapse, generating several metastable transition compounds (such as gamma and theta aluminas), cracks and mesoporosity (pores with average diameters of 2 to 50 nm) on the surface of the recently decomposed particles [30]. The combination of these two

Alumina phases:	$Al(OH)_3$		η-Al_2O_3		γ-Al_2O_3		δ-Al_2O_3		θ-Al_2O_3		α-Al_2O_3
Transformation:		→ 250–500 °C		→ 500–600 °C		→ 600–800 °C		→ 800–1000 °C		→ > 1000 °C	

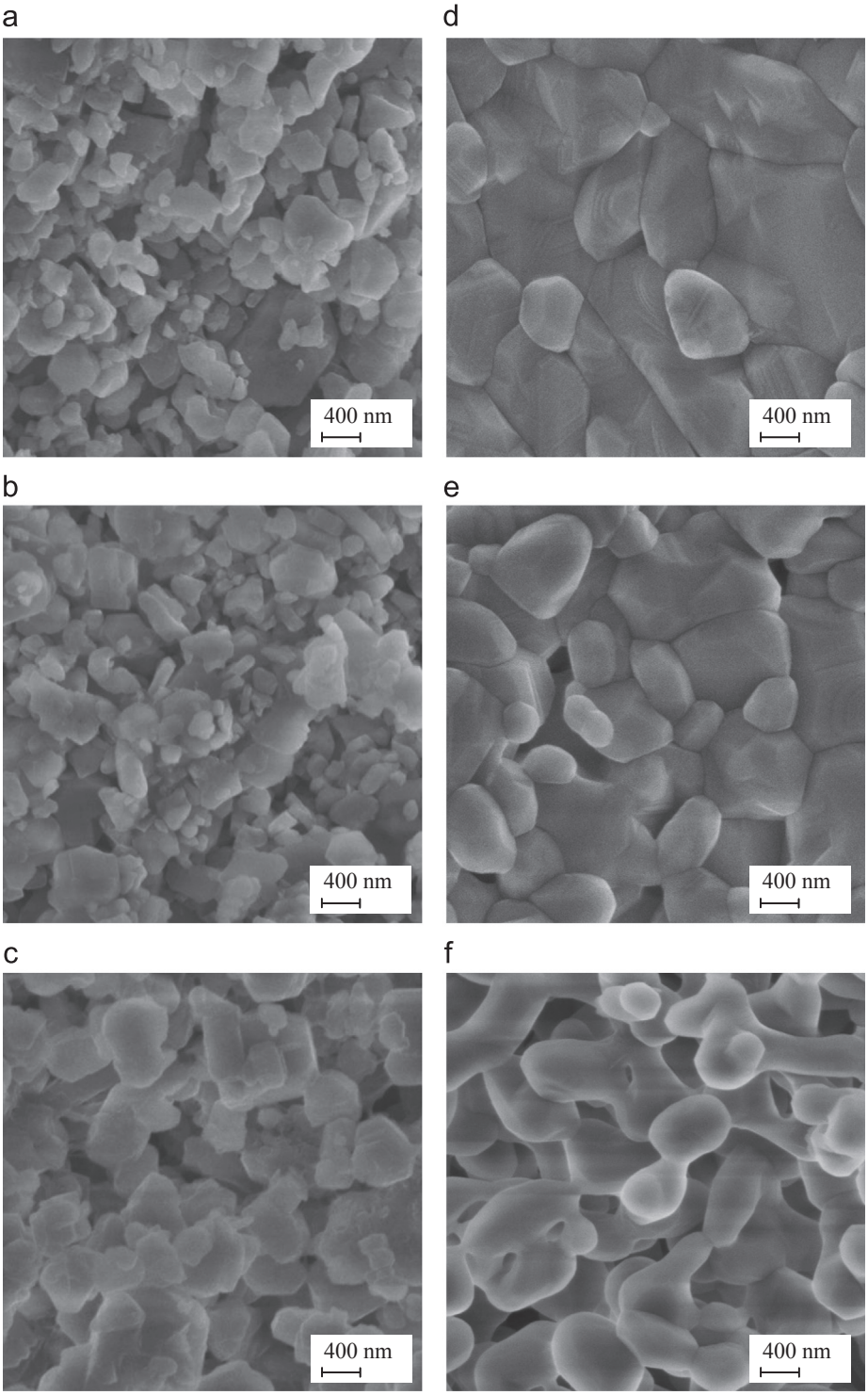

Fig. 8. Cross-section of the CA–chitosan, AH–chitosan and CA–AH–chitosan (050CA050HA sample) fibers: dried green (a, b, and c) and fired at 1500 °C (d, e, and f).

effects explains why higher $Al(OH)_3$ contents generate higher IntraP porosity (Fig. 7a) and SSA (Fig. 9a) levels at the same sintering temperature. As the temperature rises to above 600 °C and early stages of sintering take place, more stable phases are formed and transition alumina mesopores tend to disappear, reducing the porosity and the SSA [19,20,23].

3.2.2. *Interfiber porosity and mechanical strength*

The densification of the fibers (reduction of IntraP, Fig. 7a) caused two effects: (1) Reduction of total porosity (Fig. 7a) and increased volumetric shrinkage (Fig. 7b) as a function of sintering temperature; and (2) a slight increase in the contribution of interfiber porosity to total porosity (InterP, Fig. 7b). Therefore, as the sintering temperature increases and the fibers become denser and thinner, their average interfiber space increases. It is also worth noting that the AH content played a minor role in interfiber porosity, probably because this parameter considers the fibers' external geometry.

Significant differences were observed in the mechanical strength of macroelements upon varying the sintering temperature and AH content (Fig. 9b). The 100AC–000AH and 050AC–050AH samples showed sufficient mechanical strength for cup drilling and grinding, which was comparable to that of other porous structures found in the literature (considering similar apparent density [4]). On the other hand, the 000CA–100AH compositions were very brittle due to their high levels of intrafiber porosity (Fig. 8f).

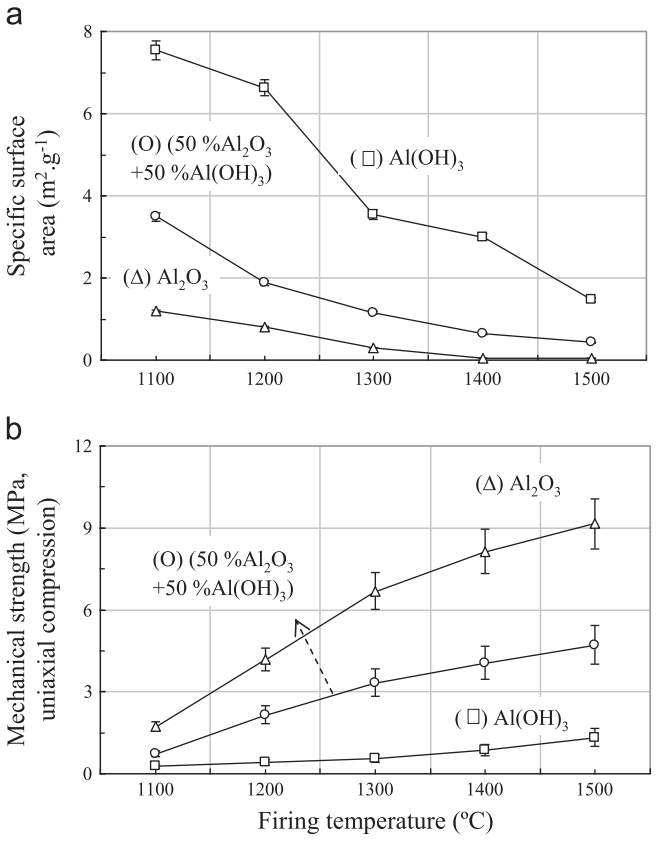

Fig. 9. (a) Specific surface area (SSA) and (b) mechanical strength (uniaxial compression) of the macroelements fired at different temperatures.

4. Final remarks

A filamentous structure with hierarchically organized pores was developed from Al_2O_3–$Al(OH)_3$–Chitosan fibers. Calcined alumina (CA), aluminum hydroxide (AH) and chitosan were codispersed successfully in 0.1 M acetic acid solution due to the compatibility of electric charges and chemical similarity between the solid particles (similar zeta potential versus pH behaviors). During wet spinning, the abrupt change in pH in the NaOH bath caused the suspensions to coagulate and chitosan molecules to precipitate rapidly on the surface of the solid particles, restricting their mobility. The continuous fibers resulting from this process were compacted and filamentous macroelements ($40 \times 40\ mm^2$ cylinders) were produced and sintered. Different levels of intrafiber (IntraP) and interfiber porosity (InterP), specific surface area (SSA), mechanical strength (MS) and volumetric shrinkage (VS) were generated by varying the CA/AH ratio and sintering temperature. Samples with higher CA content fired at higher temperatures showed lower porosity and SSA and higher MS, without significant VS. On the other hand, the addition of AH reduced the MS and increased the porosity, SSA and VS. After AH dehydroxylation, the removal of free water and increase in particle density enabled the formation of a large pre volume and transition alumina phases with high SSA and reactivity. Consequently, the driving forces for pore generation, densification and volumetric shrinkage establish a balance that can be altered intentionally by changing the composition and varying the temperature. These tunable properties and the fact that large macrostructures can be produced using these fibers highlight the technological appeal of this system for biological scaffolds, filter element and catalyst support applications.

Acknowledgments

The authors would like to acknowledge the Brazilian Research Foundations FAPESP and CNPq for supporting this research and Almatis (Brazil and Germany) for kindly supplying the samples of raw materials.

References

[1] R. Lakes, Materials with structural hierarchy, Nature 361 (11) (1993) 511–515.
[2] P. Colombo, C. Vakifahmetoglu, S. Costacurta, Fabrication of ceramic components with hierarchical porosity, Journal of Material Science 45 (2010) 5425–5455.
[3] F. Schüth, K. Sing, Definitions, terminology and classification of pore structures, in: F. Schüth, K. Sing, J. Weitkamp (Eds.), Handbook of Porous Solids, Vol. I, Wiley-VCH, Weinheim, Germany, 2002.
[4] A.R. Studart, U.T. Gonzenbach, E. Tervoot, L.J. Gauckler, Processing routes to macroporous ceramics: a review, Journal of the American Ceramics Society 89 (6) (2006) 1771–1789.
[5] L.C. Palmer, C.J. Newcomb, S.R. Kaltz, E.D. Spoerke, S.I. Stupp, Biomimetic systems for hydroxyapatite mineralization inspired by bone and enamel, Chemical Review 108 (2008) 4754–4783.

[6] N. Travitzky, H. Windsheimer, T. Fey, P. Greil, Preceramic paper-derived ceramics, Journal of the American Ceramics Society 91 (11) (2008) 3477–3492.
[7] A. Herzog, R. Klingner, U. Vogt, T. Graule, Wood-derived porous SiC ceramics by sol infiltration and carbothermal reduction, Journal of the American Ceramics Society 87 (5) (2004) 784–793.
[8] C. Tallón, R. Moreno, M.I. Nieto, Synthesis of γ-Al_2O_3 nanopowders by freeze-drying, Material Research Bulletin 41 (2006) 1520–1529.
[9] A.A. Eljaouhari, R. Mller, M. Kellermeier, K. Heckmann, W. Kunz, New anisotropic ceramic membranes from chemically fixed dissipative structures, Langmuir 22 (26) (2006) 11353–11359.
[10] F. Tang, H. Fudozi, Y. Sakka, Fabrication of macroporous alumina with tailored porosity, Journal of the American Ceramics Society 86 (12) (2003) 2050–2054.
[11] J. Moon, J.E. Grau, Ink-jet printing of binders for ceramic components, Journal of the American Ceramics Society 85 (4) (2002) 755–762.
[12] H. Seitz, W. Rieder, Three-dimensional printing of porous ceramic scaffolds for bone tissue engineering, Journal of Biomedical Materials Resarch Part B: Applied Biomaterials 74 (2) (2005) 782–788.
[13] F.C.G. de Sousa, J.R.G. Evan, Tubular hydroxyapatite scaffolds, Advances in Applied Ceramics 104 (1) (2005) 30–34.
[14] S. Alkoy, H. Yanik, B. Yapar, Fabrication of lead zirconate titanate ceramic fibers by gelation of sodium alginate, Ceramics International 33 (2007) 389–394.
[15] J. Brandi, J.C. Ximenes, M. Ferreira, R. Salomão, Gelcasting alumina—chitosan beads, Ceramics International 37 (4) (2011) 1231–1235.
[16] S. Mohanty, A.P. Rameshbabu, S. Dhara, Alpha-alumina fiber with platelet morphology through wet spinning, Journal of the American Ceramics Society 95 (4) (2012) 1234–1240.
[17] R. Salomão, J. Brandi, Filamentous alumina-chitosan porous structures produced by gelcasting, in Ceramics International, In press http://dx.doi.org/10.1016/j.ceramint.2013.03.032.
[18] Z.Y. Deng, T. Fukasawa, M. Ando, High-surface-area alumina ceramics fabricated by the decomposition of $Al(OH)_3$, Journal of the American Ceramics Society 84 (3) (2001) 485–491.
[19] Y. Deng, T. Fukasawa, M. Ando, Microstructure and mechanical properties of porous alumina ceramics fabricated by the decomposition of aluminum hydroxide, Journal of the American Ceramics Society 84 (11) (2001) 2638–2644.
[20] R. Salomão, M.O.C. Villa Boas, V.C. Pandolfelli, Porous alumina-spinel ceramics for high temperature applications, Ceramics International 37 (2011) 1393–1399.
[21] I.N. Bhattacharya, S.C. Das, P.S. Mukherjee, S. Paul, P.K. Mitra, Thermal decomposition of precipitated fine aluminium trihydroxide, Scandinavian Journal of Metallaurgy 33 (2004) 211–219.
[22] J.M.R. Mercury, P. Pena, A.H. de Aza, On the decomposition of synthetic Gibbsite studied by neutron thermodiffractometry, Journal of the American Ceramics Society 89 (12) (2006) 3728–3733.
[23] W.J. Tseng, P.S. Wu, Macroporous gibbsite foams prepared from particle-stabilized emulsions using corn starch and agar as binders, Ceramics International 38 (2012) 4461–4465.
[24] S.B. Johnson, D.E. Dunstan, G.V. Franks, Rheology of cross-linked chitosan–alumina suspensions used for a new gelcasting process, Journal of the American Ceramics Society 85 (7) (2002) 1699–1705.
[25] M. Bengisu, E. Yilmaz, Gelcasting of alumina and zirconia using chitosan gels, Ceramics International 28 (2002) 431–438.
[26] M.R. Gandhi, N. Viswanathan, S. Meenakshi, Preparation and application of alumina–chitosan biocomposite, International Journal of Biological Macromolecules 47 (2010) 146–154.
[27] X. Wang, B. Zhang, X. Liu, J.Y.S. Lin, Synthesis of *b*-oriented TS-1 films on chitosan-modified alpha–alumina substrates, Advanced Materials 18 (2006) 3261–3265.
[28] C. Qin, H. Li, Q. Xiao, Y. Liu, J. Zhu, Y. Du, Water solubility of chitosan and its antimicrobial activity, Carbohydrate Polymers 63 (2006) 367–374.
[29] F.A. López, A.L.R. Mercê, F.J. Alguacil, A. López-Delgado, A kinetic study on the thermal behavior of chitosan, Journal of Thermal Analysis and Calorimetry 91 (2008) 633–639.
[30] T. Kogure, Dehydration sequence of Gibbsite by electron-beam irradiation in a TEM, Journal of the American Ceramics Society 82 (3) (1999) 716–720.
[31] B.K. Gan, I.C. Madsen, J.G. Hockridge, In sity X-ray diffraction of the transformation of gibbsite to alpha-alumina through calcination: effect of particle size and heating rate, Journal of Applied Crystallography 42 (2009) 697–705.
[32] I. Levin, D. Brandon, Metastable alumina polymorphs: crystal structures and transition sequences, Journal of the American Ceramics Society 81 (8) (1998) 1995–2012.